Journal of Material Cycles and Waste Management (2022) 24:642–654
https://doi.org/10.1007/s10163-021-01349-7

ORIGINAL ARTICLE

Assessment of the cementitious and microstructural characteristics of an innovative waste-based eco-cement

Trong-Phuoc Huynh[1] · **Viet-Hung Vu**[2] · **Dan-Thuy Van-Pham**[3]

Received: 7 October 2021 / Accepted: 24 December 2021 / Published online: 30 January 2022

Abstract

The cementitious and microstructural characteristics of an innovative waste-based eco-cement consisting of ground granulated blast-furnace slag (GGBFS), circulating fluidized bed combustion ash (CFA), and rice husk ash (RHA) were investigated in this study. Locally sourced CFA was employed as a crucial sulfate-rich activator, and its effect on the properties of the eco-cements was studied. Five eco-cement samples were prepared using CFA/(GGBFS + RHA) ratios of 10, 15, 20, 25, and 30%, with a constant ratio of RHA/GGBFS. Results showed that increasing CFA prolonged setting time in the eco-cement. At later curing ages, the eco-cements activated by 15% CFA (CFA15) recorded higher compressive strength, dynamic moduli, ultrasonic pulse velocity, and lower drying shrinkage values than the other eco-cements. Moreover, increasing CFA to 30% decreased compressive strength by about 16%. Besides, a significant difference was found between the microstructure of CFA15 and those of the other eco-cements, which comprised C–S–H/C–A–S–H gels, ettringite, $Ca(OH)_2$, and $CaCO_3$ as their principal hydration products. Interestingly, the smallest distance between individual C–S–H and C–A–S–H layers and the intergranular fracture surface was observed in CFA15. Consequently, the X-ray diffraction patterns of CFA15 verified the increase in C–A–S–H, which is responsible for mechanical strength. This study provides further evidence for the promising potential of using CFA, GGBFS, and RHA to produce sustainable eco-cements.

Keywords Eco-cement · Drying shrinkage · Compressive strength · Dynamic moduli · Microstructure

Introduction

The construction industry is a significant contributor to gross domestic product (GDP) worldwide. While raw, site-based construction activity typically accounts for 3–10% of national GDP, this percentage rises significantly to 10–30% of national GDP when the broader construction supply network is also included [1]. The extensive use of cement-based concrete in infrastructure development and industrialization/urbanization is a major source of environmental damage and pollution in developing countries. Concrete is second only to water as the most consumed material in the world. Ordinary Portland cement (OPC) is the most common type of cement used in the manufacture of concrete. Producing cement requires significant energy inputs and is a significant source of global carbon dioxide emissions [2–4]. Thus, adjusting or altering the ingredient materials commonly used in cement production offers the potential to improve construction industry sustainability and reduce costs while optimizing levels of product quality. Sustainability has been an increasingly important goal of the construction industry worldwide since the 1980s.

In recent years, rising concerns related to environmental issues and sustainable development have broadly encouraged incorporating waste industrial/agricultural products in construction materials. Various supplementary cementitious materials (SCMs), as well as chemical agents, are common activators used in green binders (eco-cements) that are intended to replace OPC in concrete [4] through the

✉ Trong-Phuoc Huynh
htphuoc@ctu.edu.vn

[1] Department of Civil Engineering, College of Engineering Technology, Can Tho University, Campus II, 3/2 Street, Ninh Kieu District, Can Tho City 900000, Vietnam

[2] Faculty of Civil Engineering, Campus in Ho Chi Minh City, University of Transport and Communications, No. 450-451 Le Van Viet Street, Tang Nhon Phu A Ward, Thu Duc City, Ho Chi Minh City, Vietnam

[3] Department of Chemical Engineering, College of Engineering Technology, Can Tho University, Campus II, 3/2 Street, Ninh Kieu District, Can Tho City 900000, Vietnam

geopolymerization of silica and alumina-rich materials at high pH/alkaline environments. Using SCMs as an additive or partial replacement in cement has been well established to significantly improve the workability, strength, and durability of the resulting concrete; decrease production costs; provide environmental benefits via pozzolanic and hydraulic activities and the physical filling effect [5]. Besides, Scrivener et al. [6] reported that industrial by-products such as ground granulated blast-furnace slag (GGBFS), fly ash, and other naturally sourced, poorly crystalline siliceous, and reactive amorphous pozzolans may be used as SCMs in eco-cement production. These SCMs may be used individually or in combination to produce viable eco-cements for the construction industry.

GGBFS, composed mainly of SiO_2, CaO, and Al_2O_3, is a widely available by-product of the steel manufacturing process. The potential of using GGBFS as the main precursor in eco-binder used to produce self-consolidating concrete and no-cement mortars has been previously investigated [7, 8]. Circulating fluidized bed combustion ash (CFA), containing a high content of CaO and SO_3, is a by-product of clean-coal power generation systems. The high CaO and SO_3 contents make CFA to be remarkably different from the conventional fly ash, which normally comprises SiO_2, Al_2O_3, and Fe_2O_3 as major chemical compositions [9, 10]. Based on the characteristics, previous studies have suggested that fly ash can be used commonly as an SCM [9, 11, 12], while CFA can be used suitably as a sulfate-rich activator in eco-cements [13–16]. The potential utilization of CFA as a sulfate-rich activator in high-volume slag cement has been found by Lee et al. [13]. However, the feasibility of using CFA in construction materials is limited by the difficulty of separating gypsum from fly ash and the subsequent expansion in the volume of these materials [14, 17]. Therefore, the amount of CFA in cement-based materials should be controlled below 20% [15]. Nguyen et al. [16] reported that cementless paste and mortar samples made using 80% GGBFS and 20% CFA achieved a compressive strength value of 45 MPa at 28 days of curing age. In addition, after investigating the microstructure of hydrated binders, an equation was proposed to predict the compressive strength of cementless binder concrete with special consideration on the curing age and water/binder ratio. Rice husk ash (RHA), composed primarily of SiO_2, is a by-product of rice husk incineration. This ash has been recognized as a potential SCM due to its high silica content [18, 19]. However, the characteristics of RHA change with the source of rice husk and the incineration method (e.g., burning duration and temperature). Previous studies stated that the rice husk's most appropriate burning temperature was in the range of 500–800 °C, where the amorphous form of silica in RHA could be obtained. Meanwhile, oven temperatures of < 500 °C and > 800 °C, respectively, may be used to obtain the necessary organic materials and crystalline silica [20–22]. Improved strength and durability are two advantages highlighted in a previous literature review of using RHA as an SCM in cement production [23]. Moreover, the utilization of RHA is found as one of the effective ways of reducing environmental pollution and creating green and economic construction materials [24].

Based on a literature survey, commercial-scale applications of GGBFS, CFA, and RHA in the manufacture of eco-cements are currently limited, with these materials treated mainly as waste, adding to environmental pollution and landfill capacity problems. In addition, although significant research has been done on SCMs as an additive or partial replacement material in traditional OPC, minimal research into the potential of using SCMs, especially GGBFS, CFA, and RHA, as a main composite binder component has been done because of their slow reactivity, resultant toxic leachates, material quality/character variability, and other issues. Calcium–silicate–hydrate (C–S–H) and ettringite (AFt), critical to improving GGBFS strength during hydration, may be stimulated using lime and anhydrite, respectively, as alkaline and sulfate activators. Moreover, the self-cementitious properties of CFA make it a beneficial ingredient in hydraulic binders, with 15–25% CFA identified as the optimal percentage in a CFA and GGBFS mixture [25]. The engineering properties and durability of green mortars created from GGBFS, CFA, and RHA, with CFA acting as the activator, have been previously examined [26, 27], with compressive strength shown to be the highest in mortar samples containing 20% CFA and 30% RHA. Also, 120 paste samples were prepared using respective RHA/(GGBFS + RHA) ratios of 0, 15, 30, and 45% and a constant CFA/(GGBFS + RHA) ratio of 25%. It was found that samples with the waste-based eco-cement had significantly longer setting periods and compressive strength, drying shrinkage, and ultrasonic pulse velocity (UPV) values that were significantly below those in the control OPC sample. Moreover, large differences were identified using scanning electron microscopy (SEM) analysis between the microstructures of the OPC sample and waste-based eco-cements, with the high amounts of SO_3 and SiO_2 in the CFA and RHA, respectively, generating main hydration products including C–S–H and/or phase-separated Al-substitute calcium silicate hydrate (C–A–S–H) gels and AFt [4]. However, the strength-related cementitious and microstructural characteristics of an innovative waste-based eco-cement have not yet been well examined and verified, especially in terms of different CFA content ratios. Furthermore, UPV continues to be an important non-destructive testing technique that provides rapid and reliable estimations of compressive strength and dynamic modulus of elasticity (DME) using relatively inexpensive devices. So far, the evolution

of UPV and DME, as well as their correlations with eco-cement compressive strength, has yet to be well discussed in the literature sources.

In Vietnam, GGBFS, RHA, and CFA are readily obtainable as waste products [4, 28]. The innovative, waste-based eco-cement using 100% industrial solid wastes proposed in this study offers several important advantages in terms of consuming fewer natural resources and less energy in production, effectively using industrial/agricultural waste products, and extending the usable life of construction materials. In addition, this study addresses gaps in the current literature related to using readily available resources in local contexts and preliminary trial data on promising eco-cement formulations. In detail, the cementitious and microstructural characteristics of a waste-based eco-cement containing a mixture of waste materials, including GGBFS, RHA, and CFA, were investigated. The complex hydration process comprises the initial destruction of raw materials and a later polycondensation of the reaction products. Initially, an alkaline environment is created by the formation of $Ca(OH)_2$ when the CFA dissolves in water [29], with rising alkalinity in the medium accelerating the rate at which active silica and alumina sources are dissolved from the raw materials. Reactions between these sources and the Ca^{2+} and SO_4^{2-} ions generate AFt and C–S–H and C–A–S–H gels [30, 31], with these hydration products largely responsible for the increased strength levels observed in the eco-cements [7, 32]. In the chemical activation system, CFA acted as the sulfate-rich activator, while RHA was considered a high silica supplier. Based on the scopes of the study, several eco-cement samples were prepared using CFA/(GGBFS + RHA) ratios of 10, 15, 20, 25, and 30%, with constant ratios of RHA/GGBFS and water/powder at 30/70 and 40/100, respectively. These samples were used to study the role and effect of CFA content as a crucial sulfate-rich activator on the properties of eco-cements. The setting time, compressive strength, DME, drying shrinkage, and UPV of the samples were analyzed up to 91 days of curing age. In addition, microstructural analyses of the samples were performed using SEM, X-ray diffraction (XRD), and Fourier-transform infrared spectroscopy (FTIR) at 28 days of curing age. The primary objectives of this study were to (1) identify the optimal ratio of CFA dosage in ternary waste-based products; (2) propose estimated equations in terms of various UPV and DME values to predict the compressive strength of eco-cements to promote the utilization of GGBFS, RHA, and CFA as cost-effective, resource-conserving eco-cements in the construction industry; and (3) investigate the proposed eco-cements in terms of their microstructural characteristics. Study findings are expected to help advance the technological feasibility of using locally available industrial and agricultural solid-waste products (e.g., GGBFS, RHA, and CFA) in the manufacture of eco-cements.

Experimental works

Materials

In this study, a waste-based eco-cement comprising GGBFS, RHA, and CFA was supplied by local Vietnamese companies. Raw material chemical compositions and physical properties are presented in Table 1. The SEM morphology and grain size distribution, XRD patterns, and FTIR spectra of the raw materials are shown, respectively, in Figs. 1, 2, and 3. The RHA used was an industrial by-product obtained after rice husk pellets had been incinerated at temperatures of 700–900℃. As shown in Fig. 2, the silica in the RHA was in crystalline form. Therefore, the RHA used in this study exhibited relatively low pozzolanic activity, as indicated by its lower SAI value (see Table 1) compared to that of RHA used in other studies [33, 34]. Prior to use, the RHA was ground for about 2 h in a ceramic ball mill. As shown in Table 1 and Fig. 2, the GGBFS material used in this study was an amorphous cementitious material comprised mainly of SiO_2 (39.1%), CaO (37.5%), and Al_2O_3 (13%) without any clear XRD peak, while the CFA comprised mainly CaO (53.5%) and SO_3 (40.6%) and the RHA comprised SiO_2 (95.6%) primarily.

As shown in the SEM images (Fig. 1), XRD patterns (Fig. 2), and FTIR spectra (Fig. 3), the RHA used in this study was primarily crystalline silica (cristobalite) with a microporous structure, while the CFA was composed of various phases of quartz as the major crystalline, portlandite, anhydrite, and lime. Also observable in Fig. 1, the

Table 1 Physical properties and chemical compositions of raw materials

Items	GGBFS	RHA	CFA
Specific gravity, g/cm^3	2.92	2.18	2.71
Mean particle size, μm	8.8	17.4	24.9
Specific surface area, m^2/g	1.681	1.101	0.469
Loss on ignition, wt%	4.72	2.67	7.81
28-Day strength activity index (SAI), %	86.5	59.9	95.9
SiO_2, wt%	39.1	95.6	2.59
Al_2O_3, wt%	13.0	–	0.77
Fe_2O_3, wt%	0.23	0.24	0.48
CaO, wt%	37.5	0.7	53.5
MgO, wt%	7.12	–	1.21
SO_3, wt%	1.99	0.15	40.6
P_2O_5, wt%	–	0.52	0.03
TiO_2, wt%	–	0.02	–
Na_2O, wt%	–	–	0.05
K_2O, wt%	0.22	2.66	0.33

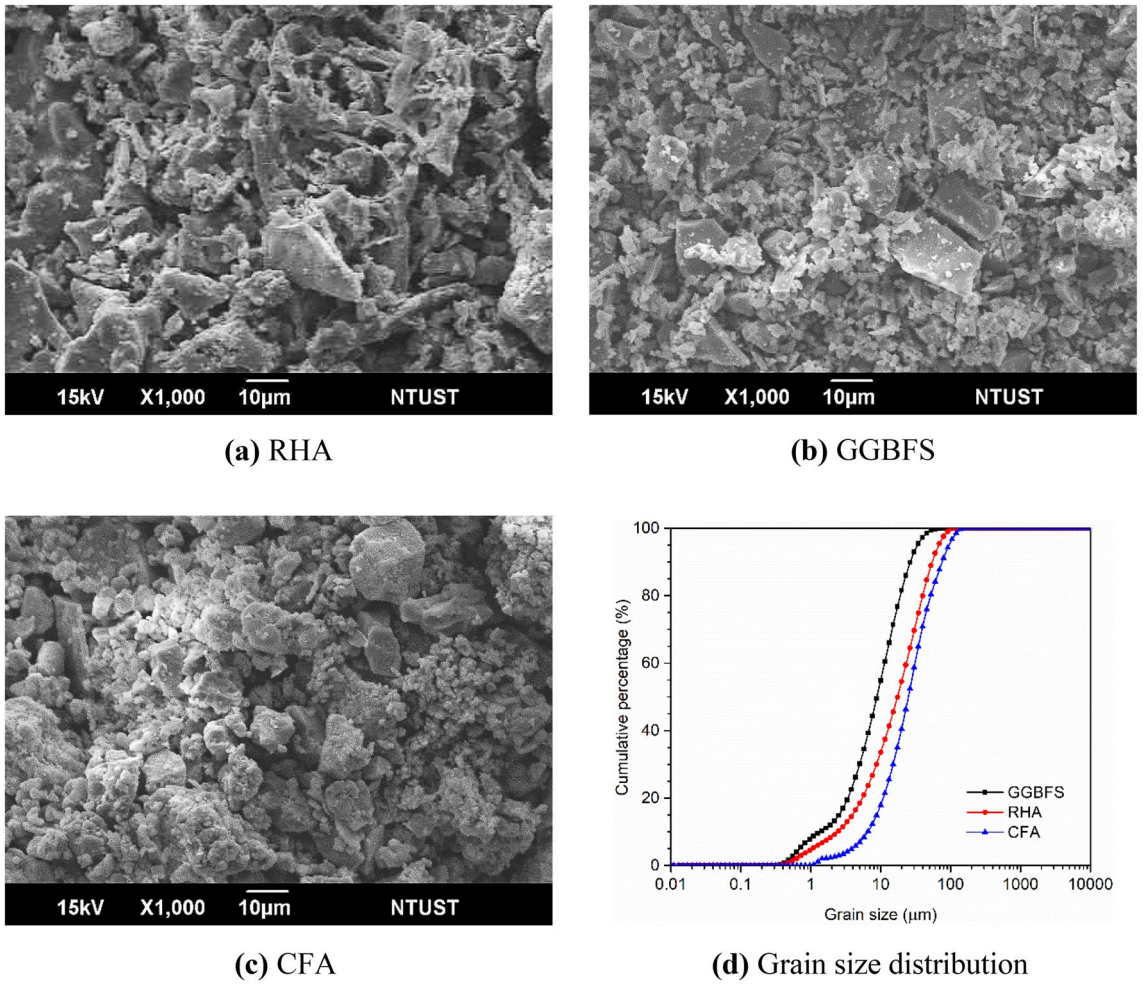

Fig. 1 SEM morphologies and grain size distribution of raw materials

RHA particles were irregular in shape, which may have allowed the active RHA with very fine particle size to act as SCMs, while the less active RHA particles to play as micro-filters in the eco-cement system. Additionally, the particle size of GGBFS was found to be the smallest among the eco-cement components, while the CFA had the coarsest mean particle size. It is worth noting that the RHA had the smallest specific gravity of the three industrial/agricultural waste products because of its highly porous structure [33]. As illustrated in Fig. 3, the peaks in the 3643–3365 cm^{-1} range are attributable to the O–H stretching vibration in the water that was absorbed within the raw materials. The signals in the 1446–1425 cm^{-1} and 873 cm^{-1} ranges were associated with the formation of calcium carbonate in CFA and GGBFS. Concurrent with the data in Table 1, no peak in these regions was observed for RHA because of its very low calcium content. The peaks in the 1120–1091 cm^{-1}, 790 cm^{-1}, 696–621 cm^{-1}, and 594–472 cm^{-1} ranges were associated with the characteristics of zeolites [34].

Mixture proportions

Based on the results of the preliminary laboratory trials, the eco-cements in this study were designed using a fixed water-to-powder (*w*/*p*) ratio of 0.4. Based on previous research, the optimum percentage of CFA is 15–25% in the GGBFS and CFA binder mixture [25], and the content of RHA in the mixture of eco-cement is viable up to 45% [4]. Therefore, in this study, five weight ratios of CFA (10, 15, 20, 25, and 30 wt%) were used in the RHA and GGBFS mixture, and a constant RHA/GGBFS ratio of 30/70 was used to prepare the ternary eco-cement. The mix proportions of the eco-cements are described in Table 2, with the number after CFA indicating the weight percentage of the material used in the eco-cement.

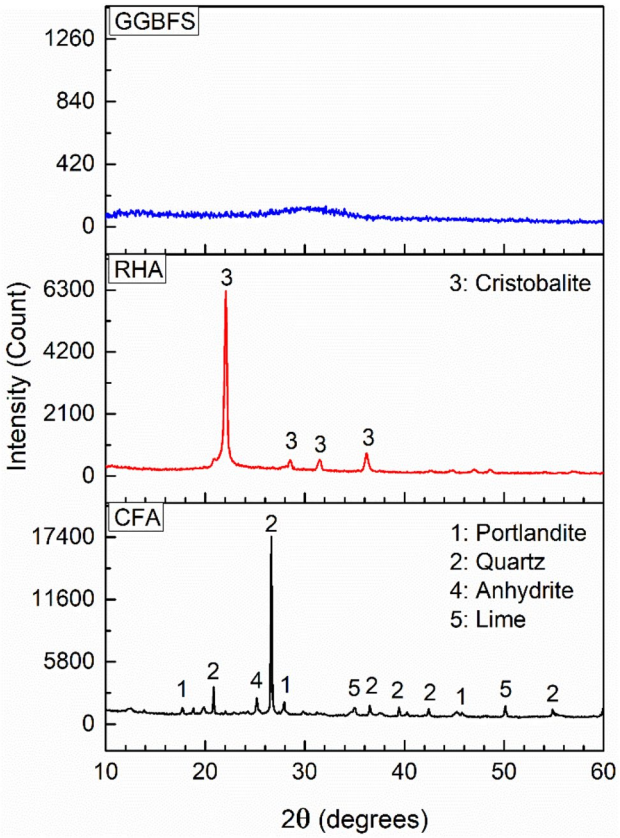

Fig. 2 XRD patterns of the raw materials

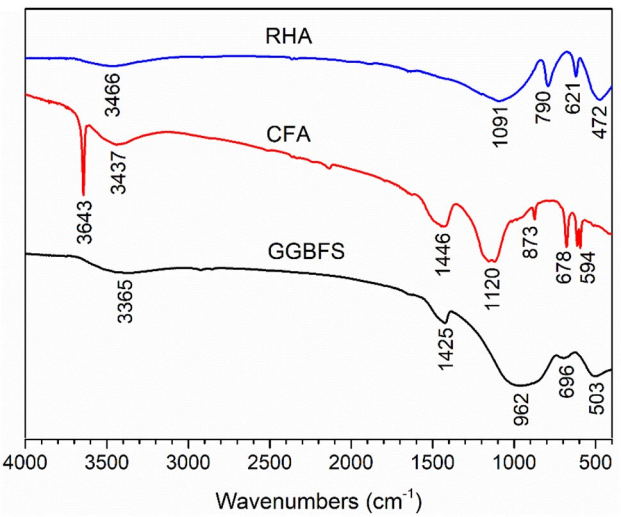

Fig. 3 FTIR spectra of raw materials

Testing methods

Setting time

Setting time is a critical fresh property for cementitious materials. In this study, the initial (IS) and final setting times (FS) for the eco-cements were checked immediately after mixing using the Vicat method in accordance with ASTM C191.

Compressive strength

The compressive strength test was performed to evaluate the strength development of the eco-cements with various ratios of CFA and the RHA and GGBFS mixture. In accordance with ASTM C109, the test was performed on cubic samples of size 50 × 50 × 50 mm at 3, 7, 14, 28, 56, and 91 days of curing age. It is noted that all of the samples were cured in the air at 25 ± 2 °C and 65 ± 5% relative humidity (RH). Compressive strength at each time point used the average of the test results for three specimens with the same CFA ratio.

Dynamic modulus of elasticity

The DME of the samples was determined in accordance with ASTM C215 at 28, 56, and 91 days of curing age using concrete cylinders measuring Ø100 × 200 mm. The eco-cements used in this test were cured in saturated lime water at 23 ± 2 °C until the testing day.

Drying shrinkage

As required under ASTM C596, drying shrinkage was measured through 91 days of curing age using prismatic paste samples of 25 × 25 × 285 mm. The de-molded samples were stored in open air (25 ± 2 °C and 65 ± 5% RH) until the testing days.

Ultrasonic pulse velocity

To assess quality and uniformity, a non-destructive UPV test was applied on several 100 mm × 200 mm cylindrical paste samples that had been cast and then air cured at 25 ± 2 °C and an RH of 65 ± 5%. The test was run at the ages of 28, 56, and 91 days following ASTM C597.

Microstructure analysis

SEM (using a JEOL JSM-6390LV), XRD (using a D2 Phaser Cu-Kα radiation diffractometer), and FTIR (using an FTS-3500 FTIR spectrophotometer) analyses were conducted on

Table 2 Compositions and setting time of the eco-cement mixtures

Mix designation	RHA (wt%)	GGBFS (wt%)	CFA (wt%)	Water/powder (wt%)	IS (min)	FS (min)
CFA10	64	27	9	40	1635	1701
CFA15	61	26	13	40	1654	1733
CFA20	58	25	17	40	1663	1758
CFA25	56	24	20	40	1669	1781
CFA30	54	23	23	40	1764	1919

Powder = (RHA + GGBFS + CFA)

28-day samples to assess their microstructural characteristics. Samples for the SEM, XRD, and FTIR analyses were obtained from specimens that had fractured during compression testing at the age of 28 days. Fragments from each eco-cement mixture were collected, submerged in methyl alcohol to halt further hydration, and dried for 24 h at 60 °C. For SEM analysis, after mounting onto an aluminum stub, each fragment was covered with a platinum–palladium alloy and vacuum dried using a 15 kV beam. For XRD analysis, the eco-cements (as prepared for SEM analysis) were ground into a powder with less than 75 µm of particle size. To identify the eco-cement phases, a step scan with an increment of 0.02° and 2θ angle of 5°–55° was performed. For FTIR analysis, a small amount of the ground powder (as prepared for XRD analysis) was mixed with KBr, set into a mold, and compressed in a cold-press machine at 4 tons of pressure to make the pellets, which were analyzed in the range of 400–4000 cm^{-1} to ascertain the hydration products.

Results and discussion

Setting time

The values of IS and FS for each eco-cement mixture are presented in Table 2. The setting times of the eco-cements were all significantly above the maximum limit of 420 min specified in ASTM C1157 and ASTM C595 for hydraulic and blended hydraulic cement. This is likely due to the high *w*/*p* ratio (0.4) in combination with slow source material reactivity [35]. As shown in Table 2, the IS and FS of CFA10 were 1635 and 1701 min, respectively, while the IS and FS of CFA15, CFA20, CFA25, and CFA30 were 1654, 1663, 1669, 1764 min and 1733, 1758, 1781, 1919 min, respectively. Moreover, although the setting time of CFA10 was 66 min, this time for CFA15, CFA20, CFA25, and CFA30 was 79, 95, 112, and 155 min, respectively. Thus, replacing traditional cementitious materials with SCMs in the binder significantly prolonged both the IS and the setting period. As previously mentioned, the delayed IS was attributed to the high *w*/*p* ratio and slow reactivity (e.g., the stable silica crystal structure in the RHA; see Fig. 1) of the SCMs in the system [35]. Moreover, the IS and FS of CFA10 were the shortest of all of the eco-cements, while CFA30 exhibited the longest setting duration (135% longer than CFA10). This may be attributed to the nature of SCMs and the lower reactivity of CFA (see Table 1) as compared to GGBFS. The outer surface of CFA particles is often enveloped by $CaSO_4$ layers [7, 36], which hinder the transport of water molecules, resulting in the low dissolution rate of CFA in the eco-cement system. Consequently, the delay in AFt formation due to the insufficient amount of SO_4^{2-} ions resulted in a longer setting time of the eco-cement mixtures [29, 37]. Moreover, increasing CFA content introduced higher SO_4^{2-} ions concentration, causing a delay in the dissolution process of $CaSO_4$ layers. As a result, the delay in chemical reactions within the system resulted in a long setting time of the eco-cement mixtures [7, 37].

Compressive strength

Compressive strength results for 3, 7, 14, 28, 56, and 91 days of curing age are presented in Fig. 4. These results indicate a relatively low compressive strength at early curing

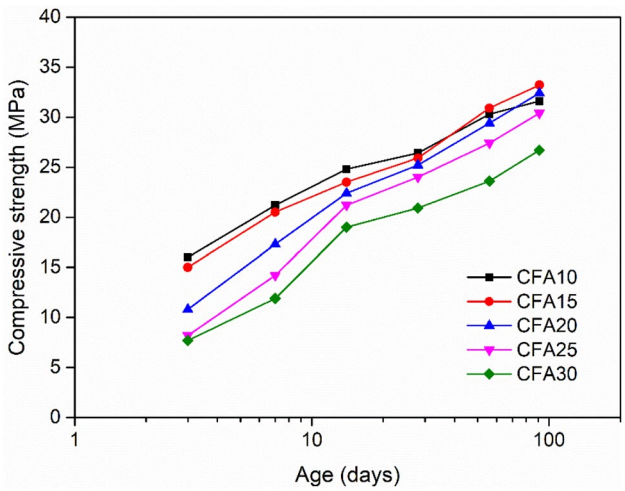

Fig. 4 Compressive strength in the eco-cement mixtures

ages. For example, the range of compressive strength values was 7.7–16 MPa for the 3-day samples and 20.9–26.4 MPa for the 28-day samples. The reduced rate of reaction of the SCMs in the blended system may explain this low early strength trend [35, 37]. However, the compressive strength increased with curing duration in all of the eco-cement mixtures regardless of CFA replacement ratio and testing age. The 91-day compressive strength values of 26.7–31.6 MPa represented a 19.7–28.2% increase in strength as compared to 28-day values. As noted in previous research [27], during the hydration, the continuous creation of AFt and C–S–H/C–A–S–H gels and further strengthens eco-cements containing waste materials.

In addition, compressive strength was significantly affected by the CFA ratio, with higher CFA ratios associated with lower levels of compressive strength, as shown in Fig. 4. The compressive strengths of CFA10, CFA15, CFA20, CFA25, and CFA30 were 26.4, 25.9, 25.2, 24.0, and 20.9 MPa, respectively, at 28 days of curing age. As previously noted, the CFA used in this study contained significant percentages of CaO and SO_3 by weight (see Table 1). These two compounds activate hydration in the waste-based binder, creating AFt and C–S–H/C–A–S–H gels, which contribute to eco-cement strength development [26, 35]. On the other hand, at 91 days of curing age, the compressive strength of the samples containing 10, 15, 20, 25, and 30% CFA content were 31.6, 33.2, 32.4, 30.4, and 26.7 MPa, respectively. Increasing the percentage of CFA reduced the percentage of GGBFS, which reduced the amounts of portlandite and alumina in samples and reduced C–S–H/C–A–S–H formation [27]. Therefore, CFA15 earned the highest 91-day compressive strength value. As shown in Fig. 4, replacing GGBFS and RHA with CFA above the 15% level significantly reduced strength. Notably, the 28-day compressive strength of CFA10, CFA15, and CFA20 were all > 25 MPa, which is the minimum compressive strength required under ACI 211.1 for civil engineering applications. Furthermore, although increasing CFA percentage reduced the mechanical strength, the compressive strength values of all eco-cement samples prepared in this study are acceptable for generally used building materials [38].

Dynamic modulus of elasticity

The DME increased with the curing age for all eco-cements, as shown in Fig. 5. However, the DME values of eco-cements varied based on the CFA replacement levels in the mixture. As seen in Fig. 5, the highest DME value was observed in CFA10 at 28 days and in CFA15 at 56 days. Also, the DME of CFA15 and CFA20 were higher than the other samples in the series at 91 days of curing age. The increase in the DME in the eco-cements was closely related to improvement in compressive strength, as shown in Figs. 4 and 5. In general, the eco-cements composed primarily of C–S–H/C–A–S–H gels and AFt had denser microstructures of hydrates due to their refined pores, which improved the DME of the eco-cements.

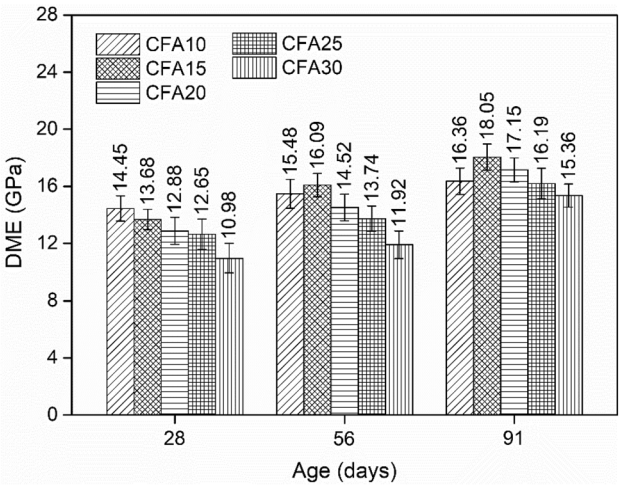

Fig. 5 DME of the eco-cement mixtures

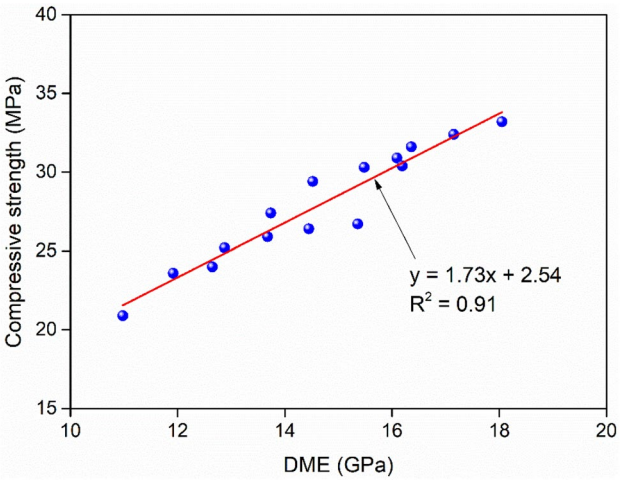

Fig. 6 DME vs. compressive strength in the eco-cement mixtures

The results of compressive strength and DME analyses on one set of eco-cements are presented in Fig. 6. The linear relationship approach has been used successfully to estimate compressive strength values by measuring the DME of eco-cements. Because a good correlation exists between the compressive strength and DME of eco-cements when CFA replacement levels in mixtures range from 10 to 30% ($R^2 = 0.91$), Eq. (1) may be applied.

$$y = 1.73x + 2.54, \tag{1}$$

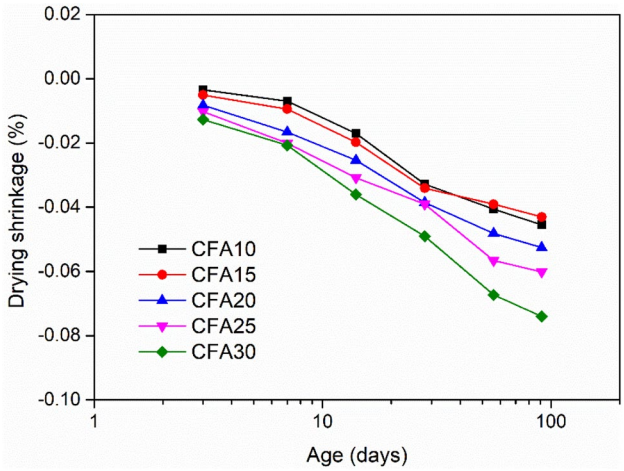

Fig. 7 Drying shrinkage in the eco-cement mixtures

where x and y are the DME and the compressive strength of eco-cements, respectively.

Drying shrinkage

Drying shrinkage in hardened eco-pastes relates directly to material durability. Drying shrinkage strain development over curing time in all of the eco-cements is shown in Fig. 7. In general, shrinkage strain increased with time, especially in samples with higher replacement levels of CFA. The result in Fig. 7 shows that CFA10 and CFA15 exhibited the smallest dry shrinkage values at all time points. For example, at 28 days, the drying shrinkage strain values for CFA10 and CFA15 were comparable (differing by 4% only). After 28 days, the values for CFA15 remained slightly (4–5%) lower than CFA10, while those samples with CFA contents above 15% reported higher levels of drying shrinkage. For instance, at 91 days of curing age, samples with CFA levels of 20, 25, and 35% had relative shrinkage values that were 122%, 140%, and 172% higher than CFA15. The significant and positive effect of RHA on eco-cement shrinkage found in this study may be attributed to the reduction in hydration reactivity, as indicated by the stable crystalline (Fig. 1) and higher microspores of RHA, which promote internal curing and reduce hydration-related heating [19, 37, 39]. In addition, the optimal ratio of CFA in CFA15 increased the volume of AFt, densifying the internal structure sufficiently to minimize free water penetration and reducing shrinkage [27]. As already mentioned in the compressive strength section, increasing the amount of CFA reduced the amount of GGBFS, which reduced the amounts of portlandite and alumina in the system and consequently reduced the formation of C–S–H/C–A–S–H [27]. As a result, the reduction in the volume of hydration products (as observed in Fig. 10) caused the changes in the mineralogical compositions of the eco-cements, introducing more pores and C–S–H/pore interfaces in the samples, allowing the penetration of free water and thus increasing drying shrinkage of the eco-cements [40–42].

Ultrasonic pulse velocity

UPV is a widely used technique for testing the internal characterization and compressive strength of cementitious composites. UPV values vary based on material density and composition. UPV values for the eco-cements in this experiment were obtained at 28, 56, and 91 days of curing age and are reported in Fig. 8. CFA10 earned the highest UPV value, with a steady decline in UPV value in all other samples, especially those with higher CFA percentages at 28 days of curing age. However, CFA15 obtained the highest UPV values over curing time. For example, at 28 days, CFA10 recorded the highest UPV value of 3181 m/s, while CFA15, CFA20, CFA25, and CFA30 each showed significantly decreased UPV values at 3092, 3052, 3001, and 2877 m/s, respectively (3–10% lower than CFA10). This may be explained by changes in the mineralogical compositions of the eco-cements reducing the volume of hydration products (Fig. 10). Thus, the presence of more pores and C–S–H/pore interfaces in the samples containing industrial by-products reduced the velocity of the ultrasonic pulse [43, 44]. The UPV results mostly confirm the compression results, with similar trends shown in Figs. 4 and 8, where higher UPV values corresponded with good quality and higher compressive strength, respectively. Furthermore, the UPV values ranged from 3061 to 3267 m/s at the 91-day, 10–30% CFA eco-cements, indicating that eco-cement mixtures incorporating waste materials meet the "medium" quality criteria outlined in BIS 13311-92 and Neville [35], proving the general applicability of these mixtures in construction.

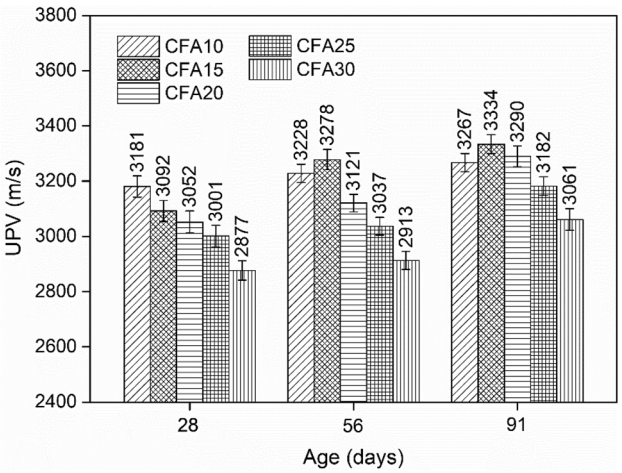

Fig. 8 UPV values of the eco-cement mixtures

In this study, the correlation between compressive strength and average UPV was established, taking into account that correlation is a statistical technique that assesses how strongly pairs of variables are related. As a linear relationship between compressive strength and average UPV was obtained (Fig. 9), Eq. (2) may be applied.

$$y = 36.29x + 2115.45, \quad (2)$$

where x and y are, respectively, the compressive strength and UPV of the eco-cements. The model fits the data well, and the analysis of the correlation coefficient ($R^2 = 0.88$) demonstrates that Eq. (2) provides an excellent estimation of eco-cement compressive strength. Moreover, the results further support using UPV as an important, non-destructive technique that provides rapid, reliable results using relatively inexpensive devices.

SEM analysis

The SEM images of the 28-day fractured samples revealed clusters embedded in the matrix (Fig. 10). This phenomenon may be explained by some of the Si being substituted by Al during the hydration of C–A–S–H and C–S–H, creating stacked layers that form compact domains. The complex matrix surrounded the C–A–S–H phases and facilitated the nucleation of C–A–S–H. It was also shown in Fig. 10 that C–A–S–H and C–S–H gels were successfully grown and a relatively denser microstructure was observed in CFA15 in comparison with other eco-cement samples. As a result, CFA15 recorded the highest density of C–S–H and C–A–S–H as well as presented the greatest adhesive characteristics, leading to the highest stiffness and hardness, which is in good agreement with the above compressive strength (Fig. 4) and UPV (Fig. 8) analysis.

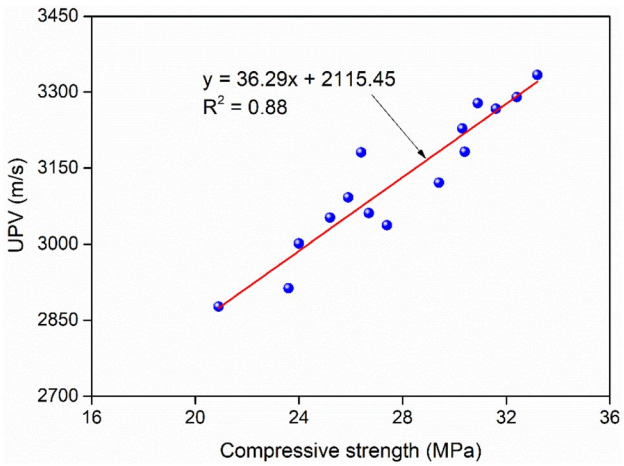

Fig. 9 UPV vs. compressive strength in the eco-cement mixtures

For further confirmation, the mole ratios of Ca/Si and Ca/Al used in this study were calculated from the chemical composition of the eco-cements (see Table 3). As increasing the CFA percentage, the Ca/Si ratio of eco-cements increased from 0.62 to 0.93, which was in the ideal range of Ca/Si ratios to form C–S–H gel assigned to the CSH3T structural model of C–S–H [45], while the Al/Ca ratio reduced from 0.31 to 0.21 (see Table 3), which was in the range of C–A–S–H formation [46, 47]. However, the structure of tobermorite-like C–S–H could not be clearly observed in the SEM images of the CFA20 (Fig. 10c), CFA25 (Fig. 10d), and CFA30 (Fig. 10e) samples. This result may suggest that the optimal Ca/Si and Al/Ca ratios in the formation of C–S–H and C–A–S–H gels in the proposed eco-cements were supposed of 0.68 and 0.28, respectively.

XRD analysis

The XRD patterns in the eco-cements are presented in Fig. 11. The phases of C–A–S–H, quartz, portlandite, and AFt were detected in all of the samples. The reaction between the dissolved Al_2O_3 (from the GGBFS) and the anhydrite and portlandite (from the CFA) produced the AFt detected in the resulting eco-cements [16]. Although the peak of C–S–H was not clearly detected in the XRD patterns of the eco-cements because of its amorphous structure [16], it is interesting that the 4-ring members of the tobermorite-like C–S–H were observable in the FTIR spectra (Fig. 12) and were thus present in the structure of the major phases. The increase in the available amount of CFA led to the decrease in the minor phases and the formation of C–A–S–H gel, which is one of the major strength contributors of the produced eco-cements (Fig. 11). This phenomenon is in line with the abovementioned compressive strength test results (Fig. 4).

FTIR analysis

The FTIR spectra for the eco-cement mixtures are presented in Fig. 12. The identical absorption bands in the FTIR spectra indicate that all of the eco-cements had similar chemical compositions, as shown in Table 4. The significant, broadbands at 3451–3402 cm^{-1} and 1653–1624 cm^{-1} indicate the respective effects of O–H stretching vibration and O–H bending on the absorbed water. The signals in the 1476–1474 cm^{-1} and the 876–874 cm^{-1} regions corresponded to calcium carbonate forming in specimens during the curing period. This is consistent with the CSH3T structural model of C–S–H [45]. The peaks in the 1151–1094 cm^{-1}, 611–606 cm^{-1}, 555 cm^{-1}, and 473–469 cm^{-1} ranges are associated with the characteristics of zeolites [34] with the contribution of Si–O–Al in C–A–S–H formation, as shown in XRD

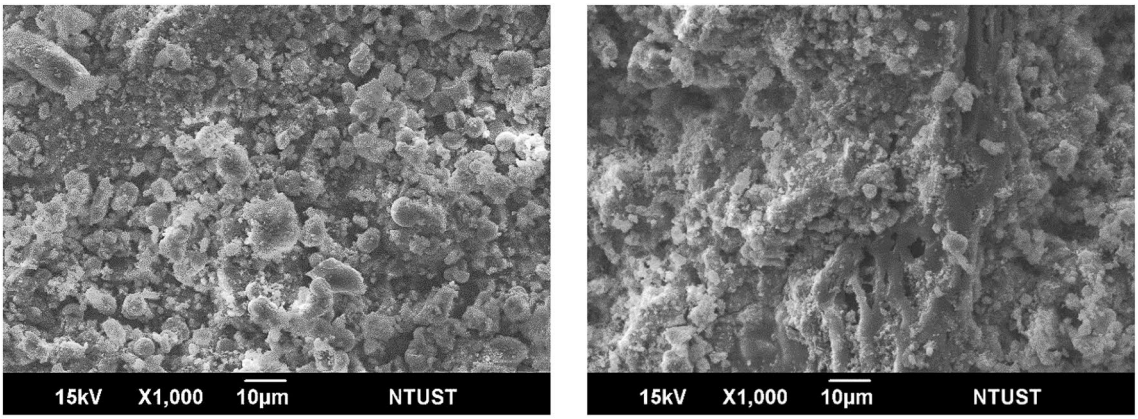

(a) CFA10 **(b)** CFA15

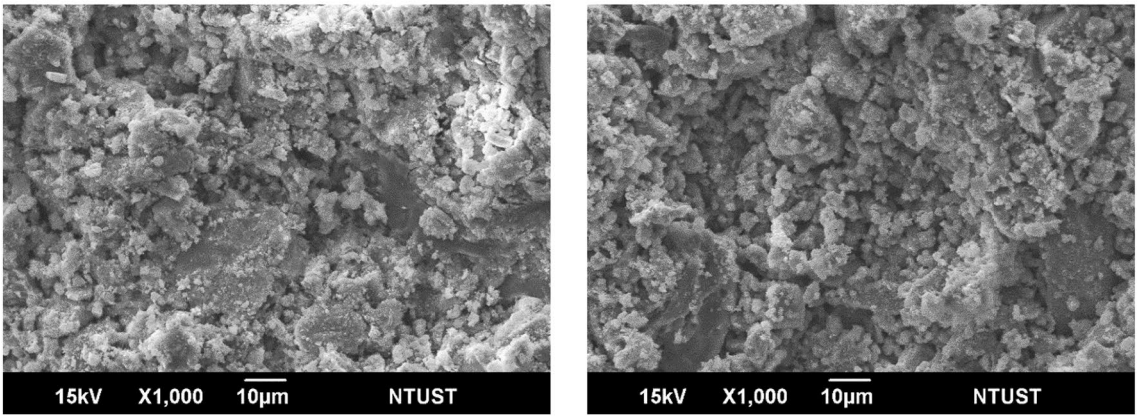

(c) CFA20 **(d)** CFA25

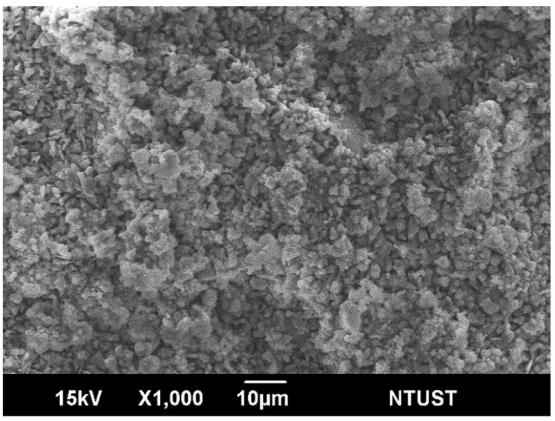

(e) CFA30

Fig. 10 SEM micrographs of the eco-cement mixtures

patterns (Fig. 11). The band at 555 cm^{-1} was reported to correspond to the symmetric stretching vibrations of the 4-membered rings in the zeolites. The results of the FTIR analysis further support $Ca(OH)_2$, $CaCO_3$, AFt, C–S–H,

Table 3 Ca/Si and Al/Ca ratios of the eco-cement mixtures

Ratios	Mix designation				
	CFA10	CFA15	CFA20	CFA25	CFA30
Ca/Si	0.62	0.68	0.75	0.83	0.93
Al/Ca	0.31	0.28	0.26	0.23	0.21

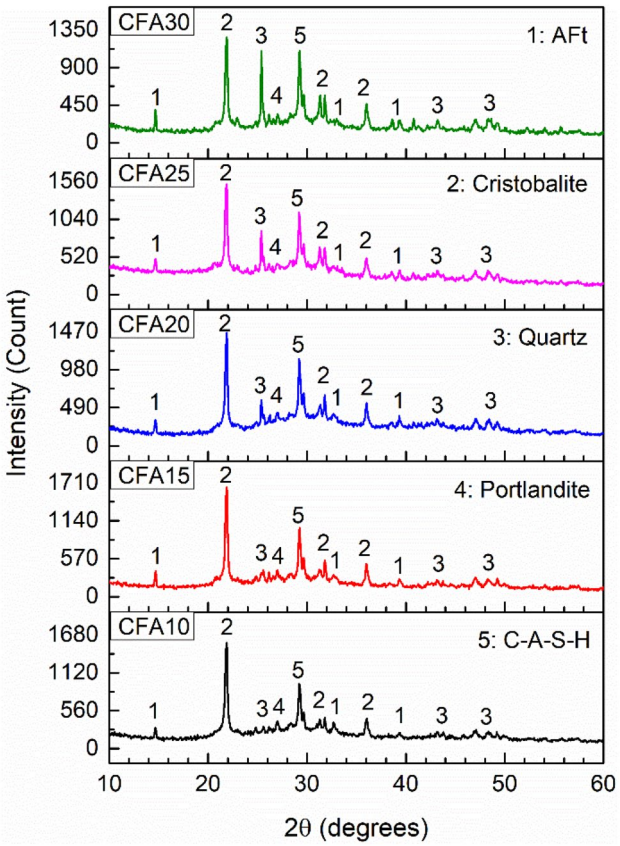

Fig. 11 XRD patterns in the eco-cement mixtures

and C–A–S–H as being the primary hydration products in the newly developed eco-cements.

Conclusions

This study took an experimental approach to investigate the role and effects of CFA content on the cementitious and microstructural characteristics of eco-cements up to 91 days of curing age. Five eco-cement samples were prepared using CFA/(GGBFS + RHA) ratios of 10, 15, 20, 25, and 30%, with a constant ratio of RHA/GGBFS. Tests were conducted to determine the setting time, compressive strength, DME, SEM, XRD, and FTIR absorption spectra. The following conclusions may be drawn based on the experimental results:

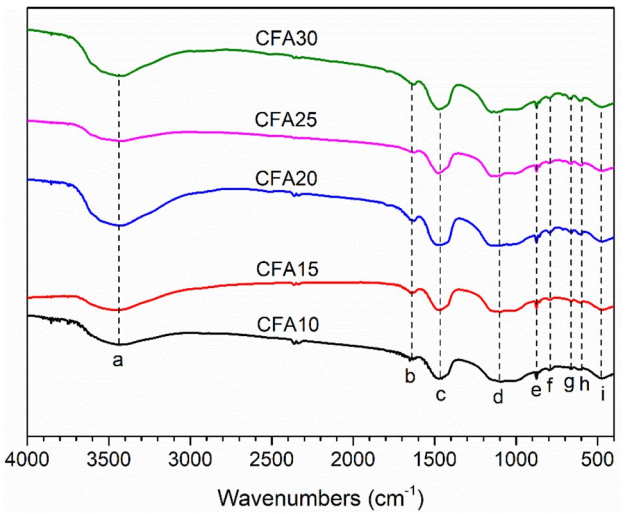

Fig. 12 FTIR spectra of the eco-cement mixtures

- The IS and FS of the eco-cement mixtures ranged between 1635 and 1764 min and 1701–1919 min, respectively. The setting time significantly increased as the percentage of CFA added to the paste mixtures increased. This may be attributed to the nature of SCMs and the lower reactivity of CFA in comparison with GGBFS, causing the delay in the chemical reactions and AFt formation and thus longer setting time.
- At later curing ages, the eco-cement activated by 15% CFA earned the highest values for compressive strength, DME, and UPV, and the lowest drying shrinkage values of all eco-cements. CFA replacement levels up to 30% exhibited decreases in compressive strength up to 16%. The maximum 91-day values for compressive strength, DME, drying shrinkage, and UPV in the eco-cement containing 15% CFA were 33.2 MPa, 18.05 GPa, − 0.043%, and 3334 m/s, respectively. These results were attributable to the reduction in GGBFS caused by the increase in CFA percentage, resulting in less portlandite and alumina in samples and consequently reducing C–S–H/C–A–S–H formation, which negatively affected the compressive strength, DME, UPV, and drying shrinkage of the eco-cements.
- Although increasing the CFA percentage over 15% reduced the mechanical strength of the eco-cements, all samples prepared in this study earned the acceptable strength values for generally used building materials. It means that the CFA/(GGBFS + RHA) ratio of 30% still could be used for producing eco-cements with a constant RHA/GGBFS ratio. With this proportion, the eco-cement samples (CFA30) at 28 days had the compressive strength and UPV values of 20.9 MPa and 2877 m/s, respectively.

Table 4 FTIR absorption bands for the functional groups of the eco-cement mixtures

Bands	Peak assignment	Peak frequency (cm^{-1})				
		CFA10	CFA15	CFA20	CFA25	CFA30
a	O–H stretching	3437	3451	3433	3402	3429
b	O–H bending	1653	1636	1636	1624	1624
c	C=O stretching (CO_3^{2-})	1474	1474	1474	1476	1474
d	Si–O(Si) and Si–O(Al) stretching	1094	1097	1097	1151	1119
e	C=O bending (CO_3^{2-})	876	876	876	876	874
f	Si–O–Si stretching	795	795	795	795	797
g	Si–O–Al stretching	606	606	606	606	611
h	Si–O–Si stretching and O–Si–O bending	555	555	555	555	555
i	O–Si–O bending	473	469	473	469	473

- A good linear correlation was found between compressive strength and UPV and between compressive strength and DME, supporting that these two tests provide an excellent estimation of compressive strength in eco-cements.
- Based on the microstructural analysis, the primary hydration products of the eco-cements included C–A–S–H and C–S–H gels, AFt, $Ca(OH)_2$, and $CaCO_3$. SEM observation revealed that the microstructure of the CFA15 was relatively denser than other samples. In addition, the XRD patterns of CFA15 corroborated an increase in C–A–S–H, which increased mechanical strength in the eco-cements. Moreover, the findings regarding the FTIR spectra were consistent with the CSH3T structural model of C–S–H with the contribution of Si–O–Al in C–A–S–H formation.
- The experimental outcomes further demonstrate the promising potential for using ternary mixtures of industrial/agricultural by-products as sustainable no-cement binders in the construction activities, especially in applications requiring lower strength thresholds and/or not requiring early high strength development. Furthermore, to promote the application of the proposed eco-cements as a building material in real practice, shortening the setting time of the eco-cements is an issue that deserves further investigation.

References

1. Hampson K, Kraatz JA, Sanchez AX (2014) The global construction industry and R&D. In: Hampson DJ et al (eds) R&D investment and impact in the global construction industry. Taylor & Francis, London. https://doi.org/10.4324/9781315774916
2. Kurokawa D, Nakaguchi A, Hirano Y, Iida T, Mori T, Matsuzawa K, Sakai E (2021) Effects of a composition change of ordinary Portland cement on waste utilization and CO_2 emissions in Japan. J Mater Cycles Waste Manag 23:1270–1275. https://doi.org/10.1007/s10163-021-01177-9
3. McLellan BC, Williams RP, Lay J, van Riessen A, Corder GD (2011) Costs and carbon emissions for geopolymer pastes in comparison to ordinary portland cement. J Clean Prod 19(9–10):1080–1090. https://doi.org/10.1016/j.jclepro.2011.02.010
4. Phuoc HT, Hung VV, Tuan BLA, Giang PHH (2020) Development of a cementless eco-binder as an alternative to traditional Portland cement in construction activities. J Sci Technol Civ Eng 14:40–52. https://doi.org/10.31814/stce.nuce2020-14(3)-04
5. Siddique R, Cachim P (2018) Waste and supplementary cementitious materials in concrete. In: Siddique R, Cachim P (eds) Waste and supplementary cementitious materials in concrete. Woodhead Publishing, India. https://doi.org/10.1016/C2016-0-04037-8
6. Scrivener KL, John VM, Gartner EM (2018) Eco-efficient cements: Potential economically viable solutions for a low-CO_2 cement-based materials industry. Cem Concr Res 114:2–26. https://doi.org/10.1016/j.cemconres.2018.03.015
7. Dung NT, Chang TP, Chen CT, Yang TR (2016) Cementitious properties and microstructure of an innovative slag eco-binder. Mater Struct 49:2009–2024. https://doi.org/10.1617/s11527-015-0630-6
8. Nguyen HA, Chang TP, Shih JY, Chen CT, Dung NT (2016) Engineering properties and durability of high-strength self-compacting concrete with no-cement SFC binder. Constr Build Mater 106:670–677. https://doi.org/10.1016/j.conbuildmat.2015.12.163
9. Ahmaruzzaman M (2010) A review on the utilization of fly ash. Prog Energy Combust Sci 36:327–363. https://doi.org/10.1016/j.pecs.2009.11.003
10. Zierold KM, Odoh C (2020) A review on fly ash from coal-fired power plants: chemical composition, regulations, and health evidence. Rev Environ Health 35:401–418. https://doi.org/10.1515/reveh-2019-0039
11. Yao ZT, Ji XS, Sarker PK, Tang JH, Ge LQ, Xia MS, Xi YQ (2015) A comprehensive review on the applications of coal fly ash. Earth Sci Rev 141:105–121. https://doi.org/10.1016/j.earscirev.2014.11.016
12. Xu G, Shi X (2018) Characteristics and applications of fly ash as a sustainable construction material: a state-of-the-art review. Resour Conserv Recycl 136:95–109. https://doi.org/10.1016/j.resconrec.2018.04.010
13. Lee HK, Jeon SM, Lee BY, Kim HK (2020) Use of circulating fluidized bed combustion bottom ash as a secondary activator in high-volume slag cement. Constr Build Mater 234:117240. https://doi.org/10.1016/j.conbuildmat.2019.117240
14. Li X, Chen Q, Ma B, Huang J, Jian S, Wu B (2012) Utilization of modified CFBC desulfurization ash as an admixture in blended cements: physico-mechanical and hydration characteristics. Fuel 102:674–680. https://doi.org/10.1016/j.fuel.2012.07.010

15. Wu T, Chi M, Huang R (2014) Characteristics of CFBC fly ash and properties of cement-based composites with CFBC fly ash and coal-fired fly ash. Constr Build Mater 66:172–180. https://doi.org/10.1016/j.conbuildmat.2014.05.057
16. Dung NT, Chang TP, Chen CT (2015) Hydration process and compressive strength of slag-CFBC fly ash materials without Portland cement. J Mater Civ Eng 27(7):04014213. https://doi.org/10.1061/(ASCE)MT.1943-5533.0001177
17. Sheng G, Li Q, Zhai J (2012) Investigation on the hydration of CFBC fly ash. Fuel 98:61–66. https://doi.org/10.1016/j.fuel.2012.02.008
18. Henry CS, Lynam JG (2020) Embodied energy of rice husk ash for sustainable cement production. Case Stud Chem Environ Eng 2:100004. https://doi.org/10.1016/j.cscee.2020.100004
19. Fapohunda C, Akinbile B, Shittu A (2017) Structure and properties of mortar and concrete with rice husk ash as partial replacement of ordinary Portland cement—a review. Int J Sustain Built Environ 6:675–692. https://doi.org/10.1016/j.ijsbe.2017.07.004
20. Mboya HA, King'ondu CK, Njau KN, Mrema AL (2017) Measurement of pozzolanic activity index of scoria, pumice, and rice husk ash as potential supplementary cementitious materials for Portland cement. Adv Civ Eng 2017:e6952645. https://doi.org/10.1155/2017/6952645
21. Thiedeitz M, Schmidt W, Härder M, Kränkel T (2020) Performance of rice husk ash as supplementary cementitious material after production in the field and in the lab. Materials 13:4319. https://doi.org/10.3390/ma13194319
22. Habeeb GA, Mahmud HB (2010) Study on properties of rice husk ash and its use as cement replacement material. Mater Res 13:185–190. https://doi.org/10.1590/S1516-14392010000200011
23. Hwang CL, Chandra S (1996) 4-the use of rice husk ash in concrete. In: Chandra S (ed) Waste materials used in concrete manufacturing. William Andrew Publishing, Westwood, pp 184–234. https://doi.org/10.1016/B978-081551393-3.50007-7
24. Thomas BS (2018) Green concrete partially comprised of rice husk ash as a supplementary cementitious material—a comprehensive review. Renew Sustain Energ Rev 82:3913–3923. https://doi.org/10.1016/j.rser.2017.10.081
25. Salain IMAK, Clastres P, Bursi JM, Pellissier C (2001) Circulating fluidized bed combustion ashes as an activator of ground vitrified blast furnace slag. Spec Publ 202:225–244. https://doi.org/10.14359/10784
26. Huynh TP, Vo DH, Hwang CL (2018) Engineering and durability properties of eco-friendly mortar using cement-free SRF binder. Constr Build Mater 160:145–155. https://doi.org/10.1016/j.conbuildmat.2017.11.040
27. Hwang CL, Vo DH, Huynh TP (2020) Physical–microstructural evaluation and sulfate resistance of no-cement mortar developed from a ternary binder of industrial by-products. Environ Prog Sustain Energ 39(5):e13421. https://doi.org/10.1002/ep.13421
28. Hwang CL, Huynh TP (2015) Investigation into the use of unground rice husk ash to produce eco-friendly construction bricks. Constr Build Mater 93:335–341. https://doi.org/10.1016/j.conbuildmat.2015.04.061
29. Anthony EJ, Jia L, Wu Y (2005) CFBC ash hydration studies. Fuel 84(11):1393–1397. https://doi.org/10.1016/j.fuel.2004.10.017
30. Schneider M, Romer M, Tschudin M, Bolio H (2011) Sustainable cement production—present and future. Cem Concr Res 41:642–650. https://doi.org/10.1016/j.cemconres.2011.03.019
31. Aprianti E, Shafigh P, Bahri S, Farahani JN (2015) Supplementary cementitious materials origin from agricultural wastes—a review. Constr Build Mater 74:176–187. https://doi.org/10.1016/j.conbuildmat.2014.10.010
32. Sandhu RK, Siddique R (2017) Influence of rice husk ash (RHA) on the properties of self-compacting concrete: a review. Constr Build Mater 153:751–764. https://doi.org/10.1016/j.conbuildmat.2017.07.165
33. Karim MR, Zain MFM, Jamil M, Lai FC (2015) Development of a zero-cement binder using slag, fly ash, and rice husk ash with chemical activator. Adv Mater Sci Eng 2015:e247065. https://doi.org/10.1155/2015/247065
34. Mozgawa W, Król M, Barczyk K (2011) FT-IR studies of zeolites from different structural groups. Chemik 65(7):667–674
35. Neville AM (2012) Properties of concrete, 5th edn. Prentice-Hall, Upper Saddle River
36. Sheng G, Li Q, Zhai J, Li F (2007) Self-cementitious properties of fly ashes from CFBC boilers co-firing coal and high-sulphur petroleum coke. Cem Concr Res 37:871–876. https://doi.org/10.1016/j.cemconres.2007.03.013
37. Chen CT, Nguyen HA, Chang TP, Yang TR, Dung NT (2015) Performance and microstructural examination on composition of hardened paste with no-cement SFC binder. Constr Build Mater 76:264–272. https://doi.org/10.1016/j.conbuildmat.2014.11.032
38. Hambach M, Volkmer D (2017) Properties of 3D-printed fiber-reinforced Portland cement paste. Cem Concr Compos 79:62–70. https://doi.org/10.1016/j.cemconcomp.2017.02.001
39. Van VTA, Rößler C, Bui DD, Ludwig HM (2014) Rice husk ash as both pozzolanic admixture and internal curing agent in ultra-high performance concrete. Cem Concr Compos 53:270–278. https://doi.org/10.1016/j.cemconcomp.2014.07.015
40. Zhang L, Qian X, Yu C, Fang M, Qian K, Lai J (2019) Influence of evaporation rate on pore size distribution, water loss, and early-age drying shrinkage of cement paste after the initial setting. Constr Build Mater 226:299–306. https://doi.org/10.1016/j.conbuildmat.2019.07.143
41. Maruyama I (2010) Origin of drying shrinkage of hardened cement paste: hydration pressure. J Adv Concr Technol 8:187–200. https://doi.org/10.3151/jact.8.187
42. Hansen W (1987) Drying shrinkage mechanisms in Portland cement paste. J Am Ceram Soc 70:323–328. https://doi.org/10.1111/j.1151-2916.1987.tb05002.x
43. An VVT (2018) The assessment of concrete quality by ultrasonic pulse velocity. J Sci Technol Civ Eng 12:20–27. https://doi.org/10.31814/stce.nuce2018-12(5)-03
44. Ali MS, Hanim MAA, Tahir SM, Jaafar CNA, Mazlan N, Matori KA (2017) The effect of commercial rice husk ash additives on the porosity, mechanical properties, and microstructure of alumina ceramics. Adv Mater Sci Eng 2017:e2586026. https://doi.org/10.1155/2017/2586026
45. Kulik DA (2011) Improving the structural consistency of C–S–H solid solution thermodynamic models. Cem Concr Res 41:477–495. https://doi.org/10.1016/j.cemconres.2011.01.012
46. Fernández R, Ruiz AI, Cuevas J (2016) Formation of C–A–S–H phases from the interaction between concrete or cement and bentonite. Clay Miner 51:223–235. https://doi.org/10.1180/claymin.2016.051.2.09
47. Hou D, Li Z, Zhao T (2014) Reactive force field simulation on polymerization and hydrolytic reactions in calcium aluminate silicate hydrate (C–A–S–H) gel: structure, dynamics and mechanical properties. RSC Adv 5:448–461. https://doi.org/10.1039/C4RA10645H